Journal of Materials Chemistry A

Solvent-Free Preparation of Imine Vitrimers: Leveraging Benzoxazine Crosslinking for Melt Processability and Tunable Mechanical Performance

Journal:	*Journal of Materials Chemistry A*
Manuscript ID	TA-ART-07-2023-004351.R1
Article Type:	Paper
Date Submitted by the Author:	25-Aug-2023
Complete List of Authors:	Hamernik, Levi; University of Southern Mississippi Guzman, William; University of Southern Mississippi Wiggins, Jeffrey; University of Southern Mississippi, School of Polymer Science and Engineering

ARTICLE

Solvent-Free Preparation of Imine Vitrimers: Leveraging Benzoxazine Crosslinking for Melt Processability and Tunable Mechanical Performance

Received 00th January 20xx,
Accepted 00th January 20xx

DOI: 10.1039/x0xx00000x

Levi J. Hamernik, William Guzman, and Jeffrey S. Wiggins*

Covalent adaptable networks, particularly imine vitrimers, have received considerable attention for the design of recyclable and reprocessable thermoset-like materials. However, the preparation of imine vitrimers often relies on solvent casting approaches that lack compatibility with existing polymer processing techniques and limit their practical application as thermoset replacements. Therefore, alternative vitrimer precursors with inherent melt processability are necessitated to realize the full potential of these recyclable materials. In this work, dynamic imine vitrimers were prepared in a solvent-free approach by employing orthogonal benzoxazine polymerizations. A series of imine-containing benzoxazine monomers were prepared to yield vitrimer precursors with tailorable rheological profiles and melt-state processability. Upon further heating, the benzoxazine functionalities undergo a condensate-free homopolymerization to yield networks with varied glass transition temperatures (34-160 °C) and impressive tensile strengths (up to 80 MPa). The incorporation of imine bonds into the backbone of the benzoxazine networks imparts efficient stress relaxations through metathesis exchange reactions, enabling malleability and repeated reprocessability at elevated temperatures. Dynamic exchange kinetics are found to be strongly correlated with crosslink density, with activation energies ranging from 70-177 kJ/mol. Additionally, we demonstrate that exposure to acidic conditions results in hydrolysis of the dynamic imine linkages, leading to full dissolution of the benzoxazine networks. This work demonstrates a solvent-free approach for preparing imine vitrimers by employing an orthogonal polymerization, and provides insight for the molecular design of processable recyclable thermosets.

Introduction

Thermoset polymers exhibit excellent mechanical properties and thermal stability, making them widely utilized in performance applications such as energy, electronics, and aerospace. However, the covalently crosslinked network structure of thermosets presents inherent challenges in recycling and repair, leading to increasing rates of waste accumulation.[1–3] Covalent adaptable networks (CANs) represent a class of polymeric materials that can undergo dynamic covalent exchanges resulting in reconfiguration of the network topology in response to external stimuli.[4,5] CANs have attracted significant attention for the design of recyclable polymers as they combine the desirable characteristics of thermosets, such as solvent resistance and mechanical strength, with the thermal processability of thermoplastics.[6–8] CANs are often broadly classified as either dissociative or associative based on the nature of their dynamic exchange mechanism. Dissociative CANs rely on thermally induced bond cleavage prior to reformation upon cooling, while associative CANs involve bond exchanges that occur through a concerted intermediate mechanism.[9,10] As such, associative networks preserve crosslink densities and retain network integrity throughout the exchange process, which prevents sudden changes in viscosity and promotes stability at elevated temperatures.[11] The field of associative CANs was initially reported by Leibler *et al.* in 2011, who demonstrated catalyzed transesterification reactions in epoxy-based networks.[12] These polymer networks, termed vitrimers, exhibited an Arrhenius-like relationship between temperature and viscosity, resulting in malleability and reprocessability reminiscent of vitreous silica.[12–14] This discovery sparked significant interest within the field, leading to the exploration of numerous alternative dynamic chemistries that enable catalyst-free bond exchange and impart improved properties such as enhanced recycling efficiency and creep resistance.[15–19]

Among the reported dynamic chemistries, imine bonds have received particular attention due to their catalyst-free associative exchange that can occur through both transamination and metathesis reactions.[20,21] Taynton *et al.* demonstrated the synthesis of imine-containing CANs through the direct condensation of multifunctional amines and aldehydes, resulting in highly crosslinked dynamic networks that exhibited thermally induced malleability and efficient reprocessability.[16,22] Additionally, imine bonds can undergo dissociative hydrolysis under acidic conditions, resulting in regeneration of starting aldehyde and amine functionalities. This degradative pathway has been leveraged to design closed-loop recyclable polymer networks.[23–26] The catalyst-free bond exchange, diverse array of aldehyde and amine precursors, and

[a] *Department of Polymer Science & Engineering, University of Southern Mississippi, Hattiesburg, Mississippi 39406, United States. Email: Jeffrey.Wiggins@usm.edu*

† Electronic Supplementary Information (ESI) available. See DOI: 10.1039/x0xx00000x

numerous pathways for recycling have resulted in imine-based dynamic networks emerging as one of the most extensively studied dynamic chemistries.[27–33] Researchers have demonstrated the ability to control thermomechanical properties and imine exchange kinetics by modifying network architecture,[34,35] hybridizing with non-dynamic engineering polymers,[36,37] and altering backbone electronic effects.[28,29] However, challenges arise in the synthesis of polyimines due to the rapid reaction of amines and aldehydes, and the water-condensate byproduct that occurs during network formation. These limitations prevent the direct, melt-state synthesis of imine networks and often necessitate solution-casting techniques using harsh solvents and lengthy drying procedures to produce vitrimer films.[37,38] To overcome these constraints, researchers have explored orthogonal reactions that enable network formation through alternative polymerization mechanisms.[39–41] For example, Stouten *et al.* developed imine-containing acrylate monomers which could undergo bulk photopolymerization and additive manufacturing to prepare void-free complex parts.[42] Imine-containing epoxides and curatives have been developed to enable network formation through condensate-free polymerizations;[43–47] however, the high reactivity of these systems still pose challenges in terms of long-term monomer storage stability and solvent-free processing. Therefore, alternative orthogonal crosslinking functionalities should be investigated to promote liquid monomer processability and enhance the properties of the resulting imine-containing networks.

Benzoxazines (BOX) are an appealing class of thermosetting materials that undergo a condensate-free ring-opening polymerization (ROP).[48,49] The synthetic simplicity of BOX monomers allows for remarkable modularity, enabling tailored molecular architectures and the incorporation of additional functionalities that can direct material properties. As a result, BOX has gained significant attention as a platform for preparing CANs.[50] Verge *et al.* employed this approach to prepare the first BOX-derived vitrimer networks that possessed rapid stress relaxation, reshapability, and reprocessability enabled by disulfide exchange.[51] This work was extended to prepare a series of bio-derived BOX vitrimers based on internally-catalyzed transesterification reactions between backbone ester bonds and pendant hydroxyl groups.[52–54] Following these initial reports of BOX-derived vitrimers, the field has grown rapidly to incorporate alternative dynamic chemistries including transacetalation,[55,56] transcarboamoylation,[57] and boronic ester exchanges.[58] Several studies have reported the incorporation of imine bonds into BOX to impart unique properties such as shape memory,[59] liquid crystalline behavior,[60] and nitrogen doping upon pyrolysis.[61] Recently, Liu et al. demonstrated the hydrolytic degradation of an imine-containing BOX network; however, the conjugated aromatic imine monomer had limited melt processability and required copolymerization with epoxides to achieve manufacturability.[60] Despite the demonstrated successful incorporation of imine bonds into BOX networks, no investigations have reported the dynamic behavior and potential recyclable characteristics of the resulting polymers.

Inspired by recent advancements in BOX-derived dynamic networks and the extensive field of imine vitrimers, this work aims to demonstrate the utilization of orthogonal BOX polymerizations to enable the solvent-free preparation of imine vitrimers. Herein, we report the synthesis of imine-containing benzoxazine monomers (iBOX) through a solvent-free condensation reaction between an aldehyde-functional BOX monomer and a series of diamines. The influence of diamine molecular weight on iBOX monomer rheological properties is investigated, demonstrating tunable viscosities and exceptional melt processability. Thermally induced crosslinking of BOX functionalities results in the formation of dynamic polyimine vitrimers that possess highly tailorable thermal and mechanical properties. The influence of crosslink density on dynamic exchange kinetics, creep performance, thermal reprocessability, and hydrolytic degradation are examined. The materials reported in this work provide insight into the molecular design of melt processable precursors that yield recyclable imine vitrimers with tailorable properties.

Experimental

Materials

4-hydroxybenzaldehyde (HBA, >99%), m-xylylenediamine (MXDA, >99%), and 1,2-bis(2-aminoethoxy) ethane (BAEE, >98%) were purchased from TCI America. Aqueous formaldehyde (Formalin, 37 wt%) and deuterated dimethylsulfoxide (DMSO-d_6, 99.96%) were purchased from Millipore Sigma Co. Benzylamine (BA >99%) was purchased from Thermo Scientific Chemicals. Polyether amines (Jeffamines D230 and D400) were purchased from Huntsman Corporation. Toluene, sodium hydroxide (NaOH), and hydrochloric acid (HCl) were purchased from Fischer Chemical. All reagents were used as received, without further purification.

Synthesis of 3-Benzyl-3,4-dihydro-2H-1,3-benzoxazine-6-carbaldehyde (HBA-BA)

Synthesis of the mono-functional aldehyde-containing benzoxazine monomer (HBA-BA) was achieved by modifying previously reported procedures.[60,62] Aqueous formalin (180 g, 2.2 mol) was added to a 1 L one-neck round bottom flask and alkalized to pH 9 using 1M NaOH. Toluene (400 mL) was added and stirred to form a heterogeneous solution prior to the dropwise addition of BA (107 g, 1.0 mol) at 25 °C. Upon full addition of BA, the reaction flask heated to 35 °C and was allowed to react for 1 h. HBA (122 g, 1.0 mol) was added to the flask and the reaction was heated to reflux and maintained for 24 h. After completion, the reaction was cooled to room temperature and the organic phase was isolated, washed with 500 mL of DI water (three times), and dried over anhydrous magnesium sulfate. The reaction solution was then concentrated to ~400 mL and placed into a refrigerator to promote crystallization. The resulting powder was collected by filtration, washed with cold toluene, and dried at 40 °C under vacuum overnight to afford HBA-BA as a white crystalline powder (218 g, 86% isolated yield, mp = 57 °C). ^{1}H NMR (600

MHz, DMSO-d6) δ 9.80 (s, 1H, -C*H*O), 7.69 (dd, J = 8.4, 2.1 Hz, 1H, C*H* aromatic), 7.60 (d, J = 2.1 Hz, 1H, C*H* aromatic), 7.38 – 7.32 (m, 2H, C*H* aromatic), 7.34 – 7.30 (m, 2H, C*H* aromatic), 7.31 – 7.26 (m, 1H, C*H* aromatic), 6.95 (d, J = 8.4 Hz, 1H, C*H* aromatic), 5.00 (s, 2H, O-CH_2-N), 4.00 (s, 2H, Ar-CH_2-N), 3.85 (s, 2H, Ar-CH_2-N). ^{13}C NMR (151 MHz, DMSO-d6) δ 191.18, 191.16, 191.13, 191.12, 159.41, 137.88, 130.16, 129.45, 129.26, 128.54, 128.33, 127.25, 120.55, 116.66, 82.91, 54.61, 48.31, 39.94, 39.80, 39.66, 39.52, 39.38, 39.24, 39.10.

Synthesis of imine-containing benzoxazine (iBOX) monomers

Preparation of the imine-containing bisbenzoxazine monomers was conducted by employing a solvent-free reaction between HBA-BA and a series of diamines. In a typical reaction, HBA-BA (30.48 g, 120 mmol) was added to a 100 mL one-neck round bottom flask and heated to 100 °C. Upon melting of the HBA-BA BOX monomer, Jeffamine D230 (15.85 g, 66 mmol) was added dropwise under vigorous stirring and left to react for 1 h. The reaction was poured into an aluminum weigh pan and was transferred to a preheated vacuum oven. The material was allowed to degas for 1h at 120 °C under reduced pressure. The material was removed and cooled to room temperature to yield D230-iBOX as a pale yellow, tacky amorphous solid (quantitative yield, T_g = 9.35 °C). ^{1}H NMR (600 MHz, DMSO-d_6) δ 8.24 – 8.06 (m, 2H, C*H*=N), 7.52 – 7.40 (m, 2H, C*H* aromatic), 7.39 – 7.32 (m, 4H, C*H* aromatic), 7.34 – 7.29 (m, 4H, C*H* aromatic), 7.31 – 7.22 (m, 2H, C*H* aromatic), 6.79 (d, *J* = 8.5 Hz, 2H, C*H* aromatic), 4.89 (s, 4H, O-CH_2-N), 3.92 (s, 4H, Ar-CH_2-N), 3.83 (s, 4H, Ar-CH_2-N), 3.55 – 3.31 (m, 8H, O- CH_2-CH), 3.37 – 3.15 (m, 4H,CH_3- C*H*-N), 1.15– 0.81 (m, 6H, CH_3- CH).

Detailed synthetic procedures for the remaining iBOX monomers are provided in the Supplementary Information. All iBOX monomers were used as prepared without further purification.

Polymerization of iBOX monomers

The iBOX monomers were heated to 120 °C and poured into preheated high temperature silicon molds of the desired test geometry. The specimens were placed in a vacuum oven and degassed at 120 °C for 1 h. The samples were transferred into an air-circulating oven preheated to 120 °C, ramped at a rate of 2 °C/min to 180 °C and held isothermally for 2 h. The samples were allowed to gradually cool to room temperature prior to demolding.

Reshaping and reprocessing of p(iBOX) networks

Reshaping of the dynamic iBOX networks was qualitatively conducted by heating in a convection oven for 5 minutes prior to forming the desired geometry and allowing to gradually cool to room temperature. Reprocessing of the materials was achieved by powderizing the cured networks using an IKA® A11 Basic Analytical Mill. Samples of the cured networks were quenched in LN2 prior to being cryo-milled at 28,000 RPM for 3 minutes to yield a fine powder with particle size < 500 μm. The powders were compression molded in a 3-piece Type V dog bone mold, using a Carver® melt press preheated to 180 °C. Samples were held under approximately 250 psi for 15 minutes.

Solvent stability and chemical Degradation of p(iBOX) networks

Solvent stability was assessed by placing samples of fully cured p(iBOX) networks into various solvents at a constant polymer concentration of 10 mg/mL. Samples were placed into an incubator oven at 25 °C for 7 days. Samples were then removed from the solvents, gently dried with a Kimwipe, and were weighed to determine mass change resulting from swelling or dissolution.

Chemical degradation was assessed by placing samples of cured p(iBOX) networks into a solution of 1M HCl and THF (1:1 v/v) at a constant polymer concentration of 10 mg/mL. Samples were held in incubator ovens at a constant temperature (25 or 50 °C). Samples were periodically removed from the solutions, surfaces were gently dried with a Kimwipe, and weighed to determine mass change. Fully depolymerized samples were diluted with DI H_2O and neutralized to pH 7 with 1M NaOH, resulting in the formation of a yellow precipitate that was isolated through vacuum filtration and dried at 75 °C under vacuum overnight.

Characterization

Nuclear magnetic resonance (NMR) spectroscopy was conducted to verify monomer structure and purity. ^{1}H, ^{13}C, COSY, HSQC, and HMBC spectra were acquired on a Bruker Ascend™ 600 MHz spectrometer (Bruker Corporation, Billerica, Massachusetts, USA). NMR samples were prepared in deuterated dimethyl sulfoxide (DMSO-d_6) at a 40 mg/mL concentration, and spectra were acquired at 303 K.

Fourier transform infrared (FTIR) spectroscopy was performed on a Perkin Elmer Frontier spectrometer (PerkinElmer Inc., Waltham, Massachusetts, USA) equipped with an Attenuated Total Reflection (ATR) accessory.

Density determination of the cured networks was achieved by employing Archimedes principle. Samples were weighed in air and in DI water at ambient temperature with a Mettler Toledo ML204 analytical balance (Mettler-Toledo, Columbus, OH)) equipped with a density determination kit.

Differential scanning calorimetry (DSC) was performed on a TA Discovery Series 2500 DSC (TA Instruments, New Castle, DE). Samples of approximately 3.0 mg of monomers or 8.0 mg of the cured networks were weighed into aluminum hermetic pans. Samples were heated in an N_2 environment from -50 to 300 °C at 5 °C/min.

Thermogravimetric analysis (TGA) was conducted on a TA Instruments Q50 TGA to assess the thermal stability of the dynamic networks. Samples were loaded onto platinum pans (~10 mg) and were subjected to a ramp from room temperature to 900 °C at 10 °C/min in both air and N_2 environments.

TGA mass spectrometry (TGA-MS) was conducted on a TA Instruments Discovery Series TGA equipped with a Discovery MS. Samples were equilibrated at 100 and heated to 325 °C at a 10 °C/min rate under an N_2 environment at a constant flow of 10 mL/min. The ion current (mA) was measured for atomic mass

units (amu) ranging from 1-100 amu to identify volatile decomposition products.

Shear rheology was performed using a TA Instruments ARES G2 rheometer, equipped with 25 mm disposable aluminum parallel plate geometry. Samples were equilibrated at their respective starting temperatures for 3 minutes prior to ramping at 1 °C/min until gelation occurred. An oscillatory strain of 1.0 % was applied at an angular frequency of 10 rad/s. Gelation temperature (T_{gel}) was measured by the crossover of storage and loss modulus.

Dynamic mechanical analysis (DMA) was conducted on a TA Instruments Q800 DMA using a tensile fixture and specimens with dimensions of approximately 30 x 5 x 1.0 mm. The samples were ramped from -100 to 220 °C at a rate of 3 °C/min with a strain amplitude of 0.05% at a frequency of 1 Hz. The T_g was measured by the peak of Tan δ.

Tensile testing was performed on an MTS Insight Electromechanical tester (MTS Systems, Eden Prarie, MN), equipped with a 2.5 kN load cell. All tests were performed in accordance with ASTM D638 guidelines using Type V dog bone specimens with a nominal gage length of 7.62 mm. All samples were tested with a minimum of five replicates.

Stress relaxation experiments were performed on a TA ARES G2 Rheometer using 8 mm parallel plate geometries with a gap of 1.0 mm. Samples of uncured iBOX were loaded onto the plates at 100 °C, heated at 2 °C/min to 180 °C, and held isothermally for 2 hours to cure the network *in-situ* directly to the parallel plates, ensuring full adhesion to the geometry, thus preventing sample slipping at the interface. SRA was conducted at 5 °C intervals between 110 and 210 °C depending on the location of the rubbery plateau. A fixed strain of 1% was applied, and the relaxation modulus (G) was monitored over 1000 seconds. After each measurement the strain was removed, temperature was increased 5 °C, and the sample was allowed to equilibrate for 10 minutes before the reapplication of strain.

Non-isothermal creep experiments were conducted on a TA Instruments Q800 DMA using a tensile fixture and specimens with dimensions of approximately 30 x 5 x 1.0 mm. A fixed tensile stress of 100 KPa was applied, and strain was monitored as samples were ramped from -100 to 240 °C at a rate of 3 °C/min. The effective vitrimer transition temperature, or topological freezing temperature ($T_{v,eff}$) was defined as the intersection of the rubbery regime tangent and the high temperature regime tangent, indicative of Maxwell fluid behavior as a result of dynamic exchange.[63]

Creep-recovery experiments were conducted on a TA Instruments Q800 DMA using a tensile fixture and specimens with dimensions of approximately 30 x 5 x 1.0 mm. Experiments were conducted at either 50 °C with a fixed tensile stress of 1 MPa, or at 150 °C with a fixed tensile stress of 0.1 Mpa. Samples were equilibrated for 5 minutes before applying the stress for a fixed 10-minute interval, followed by a 30-minute recovery period.

Thermomechanical Analysis (TMA) was conducted on a TA Q400 TMA (TA Instruments, New Castle, DE) equipped with an expansion probe. Samples of approximately 1.0 mm thickness

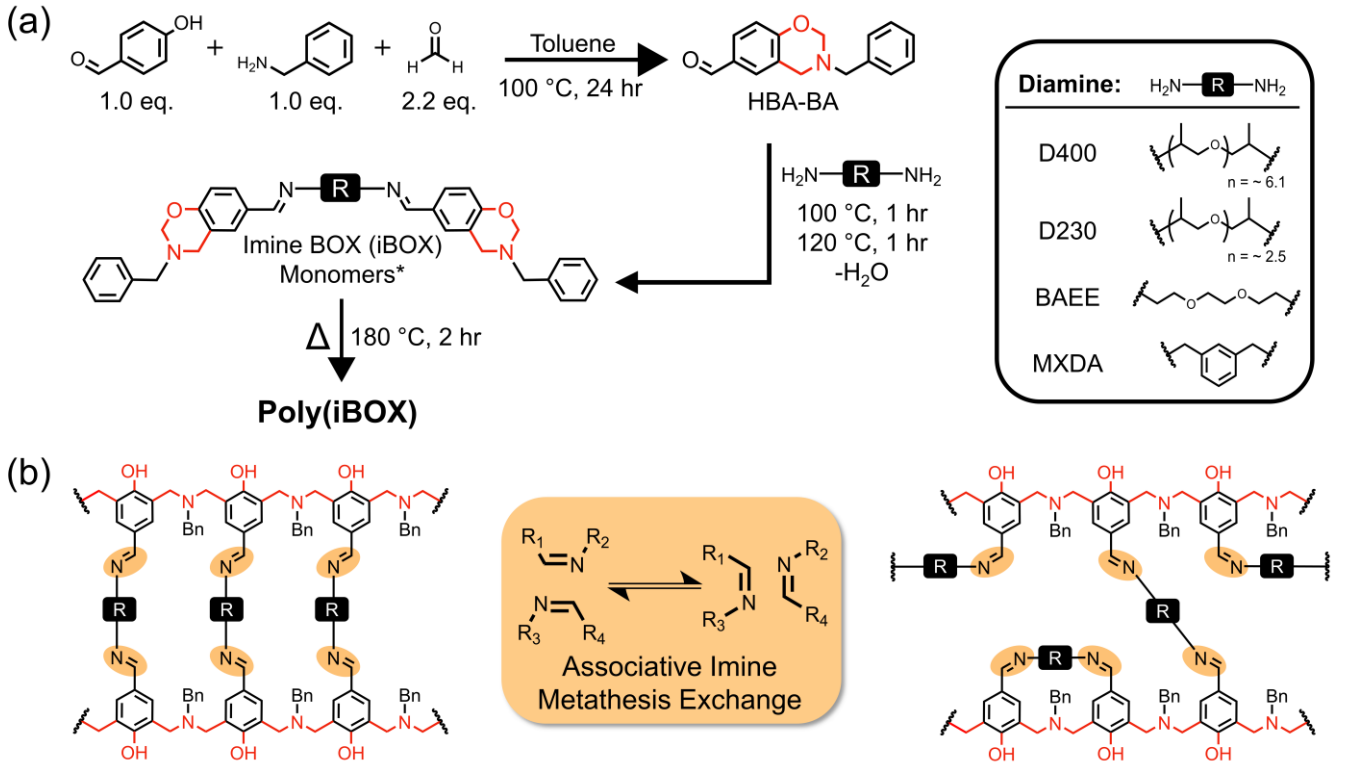

Figure 1. (a) Synthetic pathway to obtain aldehyde functionalized BOX monomer (HBA-BA) and subsequent formation of iBOX monomers* with varying diamines. (b) A fragment of the final network resulting from BOX polymerization and representation of network topology rearrangement from associative imine metathesis bond exchange (*A minor component of ring-opened species occurs in the monomer state from ring-opening addition by primary amines).

were wrapped in aluminum foil to prevent sticking to the probe and stage upon heating through $T_{v,eff}$. Samples were annealed above their respective T_g and held isothermally for 5 minutes to relieve internal stress and ensure uniform contact with the probe and stage. The samples were then equilibrated at -50 °C and a constant compressive force of 0.5 N was applied prior to ramping at 3 °C/min to 225 °C. The T_v was determined by taking the max of the dimension change curve, indicating the transition from the rubbery regime into the dynamic bond exchange regime resulting in material softening.[64]

Optical microscopy was performed to investigate the self-healing behavior of the dynamic imine-BOX networks. Samples were scratched with a fresh razor blade and were imaged using an Olympus BX53M (Olympus America, Center Valley, PA) optical microscope at 10x magnification. Samples were placed in a convection oven preheated to 180 °C and were removed for imaging at various time intervals. Crack widths were measured in Stream Essentials software, taking a minimum of five measurements across the length of the crack.

Results and discussion

Synthesis and characterization of dynamic iBOX monomers

The preparation of the melt-processable iBOX monomers was achieved through a series of condensation reactions (Fig. 1). Synthesis of the aldehyde containing BOX precursor (HBA-BA) was conducted in a one-pot reaction by reacting benzylamine (BA) with formalin at room temperature, prior to the addition of 4-hydroxybenzaldehyde (HBA). The sequential addition was necessary to preserve the aldehyde functionality for subsequent reactions. The structure and purity of the HBA-BA product was verified using ^{1}H, ^{13}C, COSY, HSQC, and HMBC NMR (Fig. 2 and Fig. S1-S5†). The ^{1}H NMR spectrum of HBA-BA exhibited characteristic benzoxazine N-CH_2-O and Ar-CH_2-O methylene bridge chemical shifts at 5.00 and 4.00 ppm, respectively. An additional methylene chemical shift was also observed at 3.85 ppm due to the benzyl CH_2 structure (Fig. 2a). Benzoxazine methylene carbons and benzyl methylene carbon chemical shifts were also observed in ^{13}C NMR at 82.9, 48.3, and 54.6, respectively (Fig. 2b). The chemical shift at 9.80 ppm (^{1}H NMR) and at 191.2 ppm (^{13}C NMR) indicated the preservation of the aldehyde functionality in the HBA-BA product.

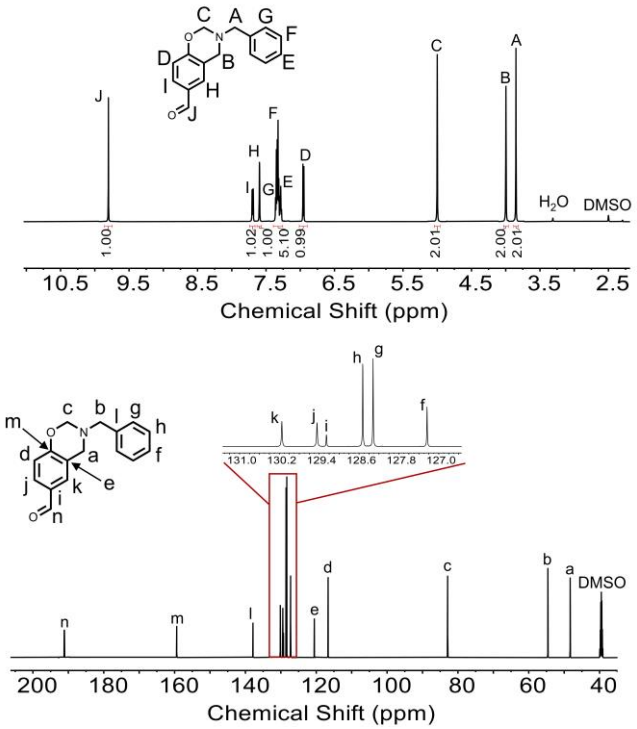

Figure 2. ^{1}H NMR spectrum (top) and ^{13}C NMR spectrum (bottom) of HBA-BA.

Synthesis of the iBOX monomers was achieved by conducting a melt-state reaction between HBA-BA and various diamines. The reaction between primary amines and the HBA-BA BOX precursor could result in two products: the desired imine-condensation with consumption of the aldehyde group, or an undesired ring-opening addition to the oxazine ring (Scheme S1).[65] Ring-opening addition reactions have been reported to be favored in aromatic amine-derived benzoxazines, which are more susceptible to nucleophilic attack by primary amines compared to stabilized aliphatic amine-based counterparts.[66] Therefore, the benzylic structure and low melting temperature of HBA-BA (T_m = 56 °C, Fig. S12†) make it an ideal precursor for minimizing ring-opening addition

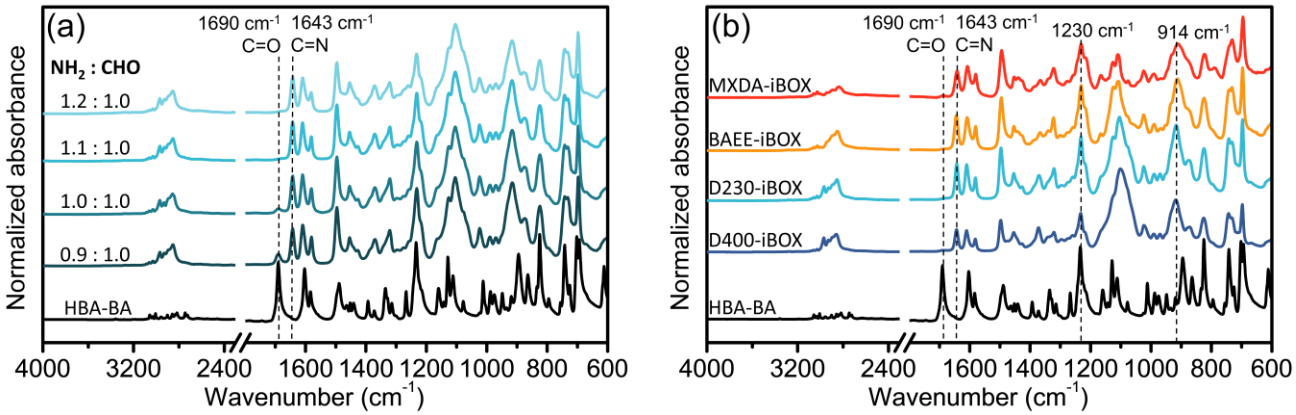

Figure 3. (a) FTIR spectra for D230-iBOX prepared with varying stoichiometry and (b) FTIR spectra of all iBOX monomers.

products and favoring imine formation under solvent-free conditions. In an initial study, the equivalencies of Jeffamine D230 and HBA-BA were varied to investigate the effect of stoichiometry on imine formation. The system that was prepared with a 10% excess of amine achieved full consumption of the aldehyde group as evidenced by the absence of the band at 1690 cm^{-1} and chemical shift at 9.80 ppm when investigated by FTIR and ^1H NMR, respectively (Fig. 3a & Fig. S6†). In all stoichiometric cases, minor evidence of ring-opening addition was observed by the appearance of a methylene chemical shift at 4.70 ppm by ^1H NMR. Relative integration of the ring-closed oxazine chemical shift at 4.89 ppm and the ring-opened chemical shift at 4.70 ppm indicated less than 5 mol% of the ring-open addition product was present. The synthesis of the remaining iBOX monomers was conducted with a fixed 10% excess of primary amines to promote full aldehyde consumption. In all systems, the aldehyde FTIR band in the HBA-BOX monomer (-CHO, 1690 cm^{-1}) disappeared (Fig. 3b), and a new characteristic imine absorbance (-CH=N- 1643 cm^{-1}) appeared. The disappearance of the chemical shift at 9.80 ppm and appearance of a new chemical shift at 8.15 ppm in ^1H NMR further confirmed the formation of the imine linkage (Fig. S7-S10†). Additionally, the characteristic asymmetric vibration of the oxazine ring (C-O-C, 1230 cm^{-1}) and the oxazine out-of-plane vibration (C-H, 914 cm^{-1}) are retained in all iBOX monomers.[67] The characteristic oxazine methylene bridge chemical shifts were also observe in all iBOX monomers in ^1H NMR (Fig. S7-S10†), confirming the retention of ring-closed benzoxazine moieties required for network formation.

DSC measurements indicated that the iBOX monomers were amorphous and possessed T_g ranging from -17 to 40 °C in contrast to the crystalline melting peak observed in HBA-BA (Fig. S11 & S12†). An exothermic peak was observed in all iBOX monomers, which was due to the thermally-activated cationic ROP of the benzoxazine functional groups.[48] The peak polymerization temperatures of the iBOX monomers ($T_{p,\ exo1}$ = 188-205 °C, Table S1†) were reduced when compared to that of the HBA-BA monomer (T_p = 215 °C). The reduction of T_p for the iBOX monomers compared to the HBA-BA monomer was attributed to the catalytic effect of phenolic species and secondary amines produced from the ring-opening addition side reaction that occurred during iBOX monomer synthesis. All iBOX monomers exhibited a secondary exothermic peak ($T_{p,\ exo2}$ = 247-252 °C) which was attributed to thermal decomposition of the resulting network following polymerization as confirmed by the abrupt mass loss observed in TGA at similar temperatures (Fig. S16 & Table S3†).

Rheological characterizations of iBOX monomers identified behavior analogous to conventional thermosetting monomers, with reductions in complex viscosity as temperature increased until the point of gelation (Fig. 4a). The T_{gel}, marked by the crossover of G' and G", was observed in each iBOX monomer to occur before 180 °C (Fig. 4b & Table S2†), and was in agreement with the trends observed in T_p measured by DSC. The reduced gelation temperature for the BAEE-iBOX was attributed to the increased reactivity of the residual, unhindered, primary amines initiating ROP at lower temperatures compared to the less

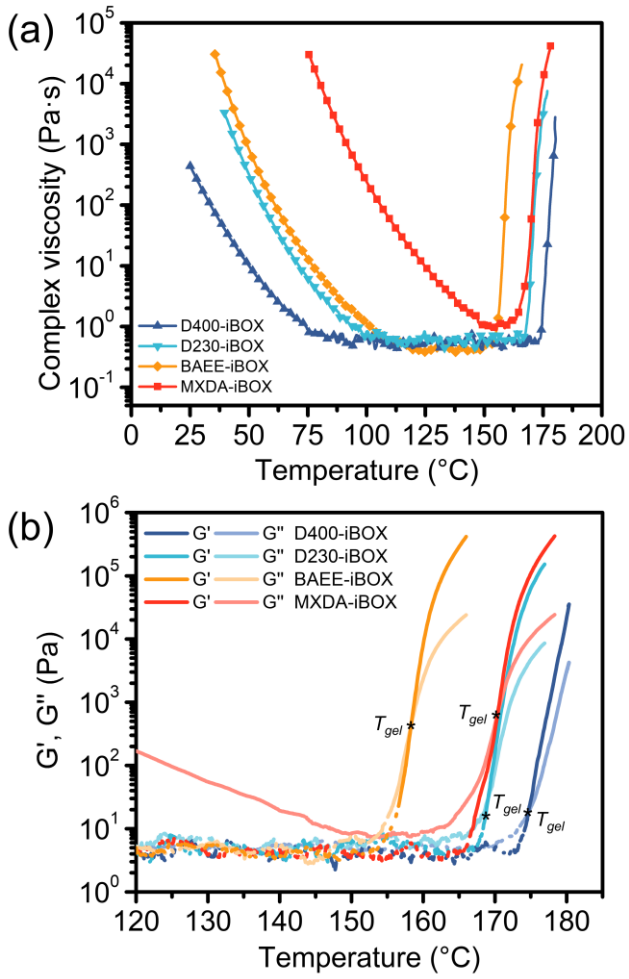

Figure 4. (a) Complex viscosity vs. temperature for all iBOX monomers and (b) gelation temperatures determine by storage and loss modulus crossover.

reactive primary amines present in the other systems. The higher molecular weight propylene oxide segment in the D400-iBOX monomer yielded a significantly lower viscosity at 50 °C compared to D230-iBOX (10.1 Pas vs 313.6 Pa·s) and a delayed onset of gelation which was attributed to the reduced concentration of reactive benzoxazine functionalities. The MXDA-iBOX possessed the highest minimum viscosity and a relatively narrow processing window due to the rigid aromatic central spacer restricting segmental mobility before the onset of polymerization. Nevertheless, all iBOX monomers were capable of being processed in the liquid state without the use of solvents.

Thermal and mechanical properties of p(iBOX) networks

The liquid iBOX monomers were polymerized isothermally in the bulk at 180 °C for 2 hours to yield homogeneous and void-free p(iBOX) networks. The DSC thermograms of each cured p(iBOX) network displayed full consumption of the first exothermic peak, indicating high degrees of ozaxine conversion (Fig. S13†). Additionally, FTIR spectra of the polymerized networks (Fig. S14†) illustrated the reduction in intensity of the characteristic oxazine absorptions at 1230 cm^{-1} and 914 cm^{-1}, further confirming that network formation was proceeding by

benzoxazine ROP.[62,67] The characteristic imine absorbance at 1643 cm^{-1} remained present in all polymerized networks, indicating that the imine bond did not interfere with the oxazine ROP and that the dynamic bonds were successfully incorporated into the resulting networks. The thermal stability of the of the resulting p(iBOX) networks ($T_{d5\%}$ ~250 °C, Fig. S16† & Table S3†) was found to be reduced compared to conventional BOX networks. TGA-MS experiments were conducted on the p(BAEE-iBOX) network to identify the primary decomposition products resulting from the initial degradation event at 250 °C. Evolved gas analysis (Fig. S19†) identified derivatives of toluene, benzylamine, and methylamine compounds, confirming that chain scission occurs at the methylene carbons of the Mannich bridge backbone segment.[68] These findings suggested that the trimethyl Mannich structure formed from the benzylamine-derived BOX networks was more susceptible to chain scission compared to the dimethyl phenyl Mannich structure that is formed in conventional aniline-derived BOX networks, resulting in the observed reduced thermal stability.[69]

The influences of the linking diamine on thermomechanical properties were investigated using DMA (Fig. 5a & Table 1). Each p(iBOX) network exhibited a uniform and monomodal Tan δ peak, indicating the formation of homogeneous networks through benzoxazine ROP. The absence of shouldering in the Tan δ peak and stable rubbery plateau modulus of each network further support the formation of fully cured networks. The p(D400-iBOX) network possessed a T_g close to room temperature (34 °C), resulting in an ambient storage modulus of approximately 300 MPa. When the diamine molecular weight was reduced, in the case of p(D230-iBOX), the T_g increased to approximately 90 °C and resulted in an ambient storage modulus nearly an order of magnitude higher (~3 GPa). When the diamine was replaced with a rigid aromatic group in p(MXDA-iBOX) the T_g increased substantially to approximately 160 °C and the ambient storage modulus increased to over 3.7 GPa. To further understand the p(iBOX) networks, the crosslink density (ν_e) of the varying networks was estimated using classical theory of rubber elasticity (eq 1).[41,70]

$$\nu_e = \frac{E'_R}{3\phi RT} \quad (1)$$

Where E'_R is the storage modulus at T_g + 30 °C, Φ is the front factor (approximated to 1.0 for an ideal rubber), R is the ideal gas constant, and T is the absolute temperature at which E'_R is taken. The expected trend of increasing crosslink density with decreasing linker diamine molecular weight was observed, with the p(MXDA-iBOX) network achieving the highest crosslink density of 3383 mol/m^3 (Table 1).

The tensile properties of the p(iBOX) networks varied significantly based on the linking diamine and the resulting crosslink density (Fig. 5b). Specifically, the p(D400-iBOX) network demonstrated impressive ductility with strains at break exceeding 250% and ultimate strength of approximately 10 MPa. The increased crosslink density of p(D230-iBOX) led to significant increases in tensile modulus and peak stress but at the penalty of ductility. As crosslink density was increased further with the p(BAEE-iBOX) and p(MXDA-iBOX) networks, the tensile modulus increased, in agreement with the storage modulus trends measured by DMA (Table 1). The highest tensile strength (79.5 MPa) was achieved with the p(BAEE-iBOX) network despite having a lower modulus than the p(MXDA-iBOX) network. The increased tensile strength resulted from increased flexibility of the ethylene oxide backbone segment in p(BAEE-iBOX) that enabled increased strain before failure compared to the rigid aromatic backbone segment in p(MXDA-iBOX). It is worth noting that even the most brittle network, p(MXDA-iBOX), possessed mechanical properties superior to many traditional monomer-derived polybenzoxazines, which often are reported to exhibit strains at break of < 5% and ultimate stress below 50 MPa.[71–73] The low mechanical properties and brittle nature of traditional BOX have been rationalized by the defects that occur during polymerization, such as intramolecular hydrogen bonding, termination of the propagating chain, and the presence of dangling chain ends that can result from vitrification.[48,74] More specifically, defects in the final polymer network will reduce the covalent connectivity, thus significantly reducing mechanical properties. The observed increase in mechanical properties of p(iBOX) networks may be rationalized by the absence of vitrification during polymerization of iBOX monomers, thus minimizing defects and

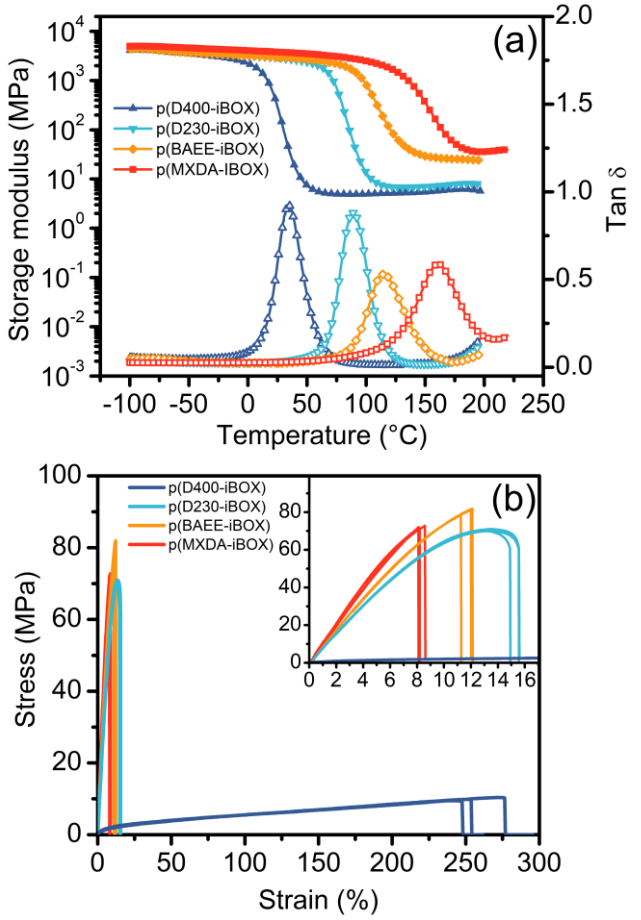

Figure 5. (a) Storage modulus and tan δ vs. temperature of p(iBOX) networks. (b) Tensile stress-strain curves of p(iBOX) networks (3 replicates shown).

Table 1. Summary of the thermal and mechanical properties of p(iBOX) networks

		DMA				Tensile Testing		
Vitrimer Network	Density (g/cm³)[a]	T_g (°C)[b]	E' at 25 °C (MPa)	E'_R (MPa)[c]	ν_e (mol/m³)[d]	Young's Modulus (MPa)	Peak stress (MPa)	Strain at break (%)
p(D400-iBOX)	1.112 ± 0.002	34.4	291.7	5.25	623	19.08 ± 3.65	9.70 ± 0.38	265 ± 14
p(D230-iBOX)	1.136 ± 0.001	88.6	2883	7.66	784	806.3 ± 21.4	70.1 ± 0.5	15.3 ± 0.6
p(BAEE-iBOX)	1.189 ± 0.002	114.8	2961	31.9	3063	883.7 ± 26.9	79.5 ± 2.1	11.9 ± 0.5
p(MXDA-iBOX)	1.186 ± 0.002	160.5	3789	39.1	3383	989.2 ± 33.0	70.3 ± 2.8	8.4 ± 0.5

[a]measured by Archimedes principle. [b]determined by the peak of Tan δ. [c]E'_R is the storage modulus from the DMA curves at T_g + 30 °C. [d]V_e is the crosslink density per unit volume.

yielding increased covalent connectivity in the resulting networks.[75] Moreover, the inclusion of flexible backbone segments and increased molecular weight between crosslinking oxazine functionalities led to reductions in the tensile modulus of the p(iBOX) networks compared to the rigid fully aromatic structures in traditional BOX, which resulted in higher strain capabilities and therefore improved toughness.

Characterization of p(iBOX) network dynamic exchange

The dynamic properties of the p(iBOX) networks were investigated by conducting stress relaxation experiments. All networks exhibited temperature dependent relaxation within short time scales (Fig. 6a and Fig. S18-S21†), which resulted from topological rearrangements occurring through dynamic imine metathesis (Fig. 1). The characteristic relaxation time (τ) was defined as the time it takes for the normalized modulus (G/G_0) to relax to a value of 1/e (≈0.37), in accordance to the Maxwell model.[28,76] The temperature dependence of the relaxation time was used to construct an Arrhenius plot, and the exchange activation energy (E_a) was determined from the linear regression, using eq 2.

$$\ln(\tau) = \frac{E_a}{RT} + \ln(\tau_0) \quad (2)$$

The exchange E_a of the p(iBOX) networks were found to range from 70 to 177 kJ/mol (Fig. 6b & Table 2) which was comparable to other reported imine metathesis-based vitrimers.[10,77] The observed trend of increased E_a with increased network crosslink density was contradictory to recent literature findings, that report reduced E_a as a results of increased dynamic bond proximity.[17,52] However, it is important to note that the exchange E_a measured through stress relaxation is an apparent value that describes the sensitivity of the material's viscosity in response to changing temperature. Therefore, the measured E_a is significantly influenced by physical parameters such as network topology and localized segmental rigidity, in addition to the underlying Ea of the chemical exchange process. This results in the observed stress relaxation time being the sum of characteristic timescales for bond exchange and functional group diffusion within the network.[63] Dynamic networks often rely on the exchange of mobile pendant functional groups, such as free hydroxyls in the case of transesterifications,[52] whereas the p(iBOX) networks rely on metathesis reactions of dynamic bonds that are incorporated directly into the network backbone. The observed increase in E_a was attributed to diffusion limitations that arose as crosslink density (and therefore viscosity) increased, requiring more energy to overcome restricted network mobility. Specifically, the highest apparent E_a, observed in the p(MXDA-iBOX) network, was a result of the rigid aromatic network backbone requiring more energy to attain sufficient mobility to achieve dynamic bond exchange compared to a more flexible backbone, such as in the polyether p(iBOX) networks.

An important thermal transition of vitrimer-like materials is the temperature at which associative bond exchange begins, resulting in network malleability. This temperature has been denoted as the topological freezing temperature (T_v) and was initially defined as the temperature at which the material's viscosity exceeded 10^{12} Pa·s.[12] Conventionally, T_v is not directly measured, and instead relies on extrapolating the stress relaxation Arrhenius plot to the relaxation time that corresponds to a viscosity of 10^{12} Pa·s. Extrapolation of the Arrhenius plots for the p(iBOX) networks resulted in low T_v values ranging from 5 to 124 °C (Table 2), all of which were below the T_g for each respective network. Advancements in vitrimer literature have noted that this extrapolation approach for measuring T_v often results in a value that has little physical significance. This is particularly relevant in the case where the estimated T_v occurs below the T_g of the network where segmental motion is effectively frozen thus preventing the diffusion and exchange of dynamic moieties.[17,63] Recent efforts have demonstrated that non-isothermal, iso-stress experiments, such as dilatometry or creep provide a physical

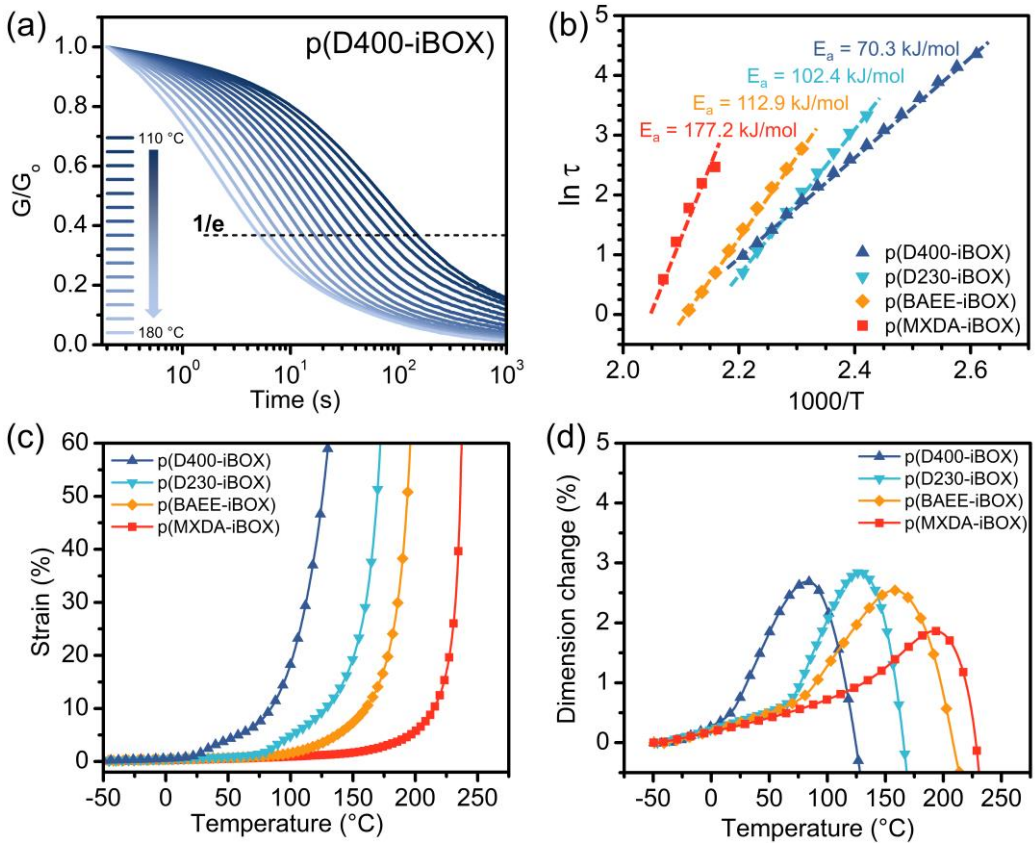

Figure 6. (a) Normalized stress relaxation curves of p(D400-iBOX) at 5 °C intervals. (b) Arrhenius plot of ln(τ) vs. 1000/T showing linear fits and corresponding activation energies of each p(iBOX) network. (c) Non-isothermal creep curves of p(iBOX) networks and (d) Normalized TMA results of p(iBOX) networks indicating dimension change as samples are heated through T_g and $T_{v,eff}$.

measurement that is a better indication of bond exchange, and clearly define an effective topology freezing temperature ($T_{v,eff}$).[63,78]

Non-isothermal creep experiments were conducted on the p(iBOX) networks, where $T_{v,eff}$ was observed as the onset of rapid tensile strain. Specifically, $T_{v,eff}$ occurred above the T_g for each respective network, following similar trends as E_a with increasing crosslink density. The two propylene oxide based networks, p(D400-iBOX) and p(230-iBOX), demonstrated the expected step change in strain associated with T_g, followed by a stable rubbery regime prior to the rapid onset of strain (Fig. 6c). Conversely, p(BAEE-iBOX) and p(MXDA-iBOX) networks didn't exhibit a rubbery regime, straining immediately upon deviating from the glassy state. The lack of rubbery regime in the p(BAEE-iBOX) and p(MXDA-iBOX) networks suggested that these materials were limited by T_g, thus the rapid bond exchange occurred immediately once segmental motion began. To test this hypothesis, we conducted thermomechanical analysis (TMA), which has recently been established as an effective method for measuring $T_{v,eff}$ under less force-dependent, compressive conditions.[64] All of the p(iBOX) networks exhibited an inflection point in dimensional change, indicating a change in the coefficient of thermal expansion (CTE) associated with T_g, prior to reaching a dimensional change maximum, associated with $T_{v,eff}$. Specifically, the maximum point of dimensional change indicated the transition from a rubbery regime into a bond exchange dominated regime that resulted in material softening and probe indentation (Fig. 6d). These findings demonstrated that the p(BAEE-iBOX) and p(MXDA-iBOX) networks did possess rubbery regimes where limited segmental mobility and diffusion constraints prevented bond exchange immediately above T_g. The $T_{v,eff}$ values measured by TMA were in agreement with the values measured by non-isothermal

Table 2. Summary of p(iBOX) dynamic properties

	Stress Relaxation		Non-Isothermal Creep	TMA
Vitrimer Network	E_a (kJ/mol)[a]	T_v (°C)[b]	$T_{v,eff}$ (°C)[c]	$T_{v,eff}$ (°C)[d]
p(D400-iBOX)	70.3 ± 0.6	4.8 ± 2.6	92.6	83.1
p(D230-iBOX)	102 ± 2	44.9 ± 7.0	144	128
p(BAEE-iBOX)	113 ± 3	71.7 ± 9.2	163	158
p(MXDA-iBOX)	177 ± 18	124 ± 13	209	194

[a]Measured from linear regression of Arrhenius stress relaxation plot. [b]Determined from extrapolating Arrhenius plot to η = 10^{12} Pa·s. [c]Measured from the onset of rapid strain in non-isothermal creep experiments. [d]Determine from the peak of dimension change measured via expansion TMA.

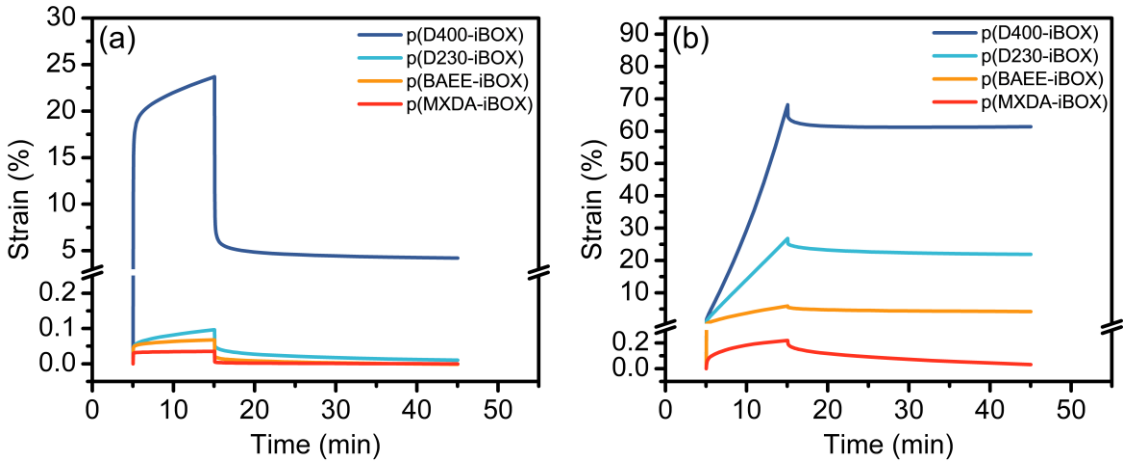

Figure 7. Creep-recovery experiment for p(iBOX) networks at (a) 50 °C at a constant tensile force of 1.0 MPa and (b) at 150 °C at a constant tensile force of 0.1 MPa.

creep for each p(iBOX) network and both methods provided a good indication for what temperature bond exchange occurs, thus identifying an effective temperature for predicting creep susceptibility and for defining reprocessing conditions.

Creep-recovery experiments were conducted at both 50 °C and 150 °C to investigate the isothermal creep resistance of p(iBOX) networks in relation to their respective T_g and $T_{v,eff.}$ The three glassy networks (p(D230-iBOX), p(BAEE-iBOX), and p(MXDA-iBOX) all exhibited minimal strain at 50 °C (< 0.2%) and creep recovery approaching 100% (Fig. 7a & Fig. S24†). These findings indicated that segmental mobility constraints of the glassy state precluded dynamic bond exchange and limited permanent deformation. The p(D400-iBOX) network, tested above T_g in the rubbery state, underwent a strain of ~25% at 50 °C, but achieved strain recovery greater than 80% (Table S5†). The high strain recovery of p(D400-iBOX) at 50 °C suggested that despite having segmental mobility, minimal bond exchange occurred below $T_{v,eff}$ and the original network architecture was largely preserved. Conversely, when tested at 150 °C, permanent deformation occurred in all polyether based (iBOX) networks, with higher extents of creep and reduced strain recovery observed in networks with reduced crosslink density (Fig.7b 7a & Fig. S25†). More specifically, the p(D400-iBOX) network exhibited a strain in excess of 60% and recovery of less than 10%, whereas the p(BAEE-iBOX) network strained less than 6% and recovered over 28%. The high T_g and $T_{v,eff}$ of the p(MXDA-iBOX) network resulted in exceptional resistance to creep even at 150 °C, exhibiting strain of less than 0.5% and recovery greater than 85% (Table S5†). The results of the creep recovery experiments demonstrated impressive resistance to permanent deformation at low temperatures and predictable creep behavior at elevated temperatures based on the measured $T_{v,eff}$ and network crosslink density. The observed creep performance of the p(iBOX) networks at elevated temperatures was comparable to similar imine vitrimers prepared through solution casting approaches, demonstrating the ability of orthogonal benzoxazine crosslinking to achieve dynamic imine networks with similar material properties.[38,79]

Malleability, reprocessing & self-healing

The dynamic bond exchange reactions that enable stress relaxation in the p(iBOX) networks also allow the materials to exhibit exceptional malleability. When the networks were heated above the $T_{v,eff}$ (determined by TMA), the samples were able to easily be deformed into the desired geometry, and locked in place once cooled below T_g (Fig. 8a). Upon reheating the samples above $T_{v,eff}$, the geometry was retained which indicated that the imparted deformation occurred through covalent reconfiguration of the network topology, and was not the result of shape memory effects driven by entropic elasticity.[80] A new geometry could be programmed by again deforming the sample at temperatures above $T_{v,eff}$, thus demonstrating the repeated reconfiguration of the network through dynamic imine exchange.

To assess the network reprocessability enabled by imine exchange, broken tensile bars were ground to a fine powder using a cryomill and then subjected to compression molding (Fig. 8b & Fig. S26†). The rapid stress relaxation afforded by imine exchange enabled rapid reprocessing times (~15 min) compared to other reported dynamic networks which can require hour(s) to achieve network reformation.[50,53] The three polyether-based p(iBOX) networks were efficiently reprocessed at 180 °C to yield uniform, transparent specimens with no discernable change to the chemical structure when examined through FTIR (Fig. S31-S34†). The high T_g of the p(MXDA-iBOX) network resulted in poor powder sintering at 180 °C, but when the temperature was increased to 200 °C (above the $T_{v,eff}$), the material formed transparent, homogenous samples.

Tensile testing of the reprocessed p(BAEE-iBOX) network demonstrated comparable stress-strain curves (Fig. 8c) with reprocessed tensile modulus, tensile strength, and elongation at break achieving 98%, 68% and 71% of the virgin material properties, respectively (Fig. 8d). The modulus retention through repeated reprocessing indicated the high degree of healing efficiency afforded by dynamic imine exchange. The observed reductions in elongation at break and ultimate strength in the glassy p(iBOX) networks are commonly reported in high T_g dynamic networks, and are attributed to the

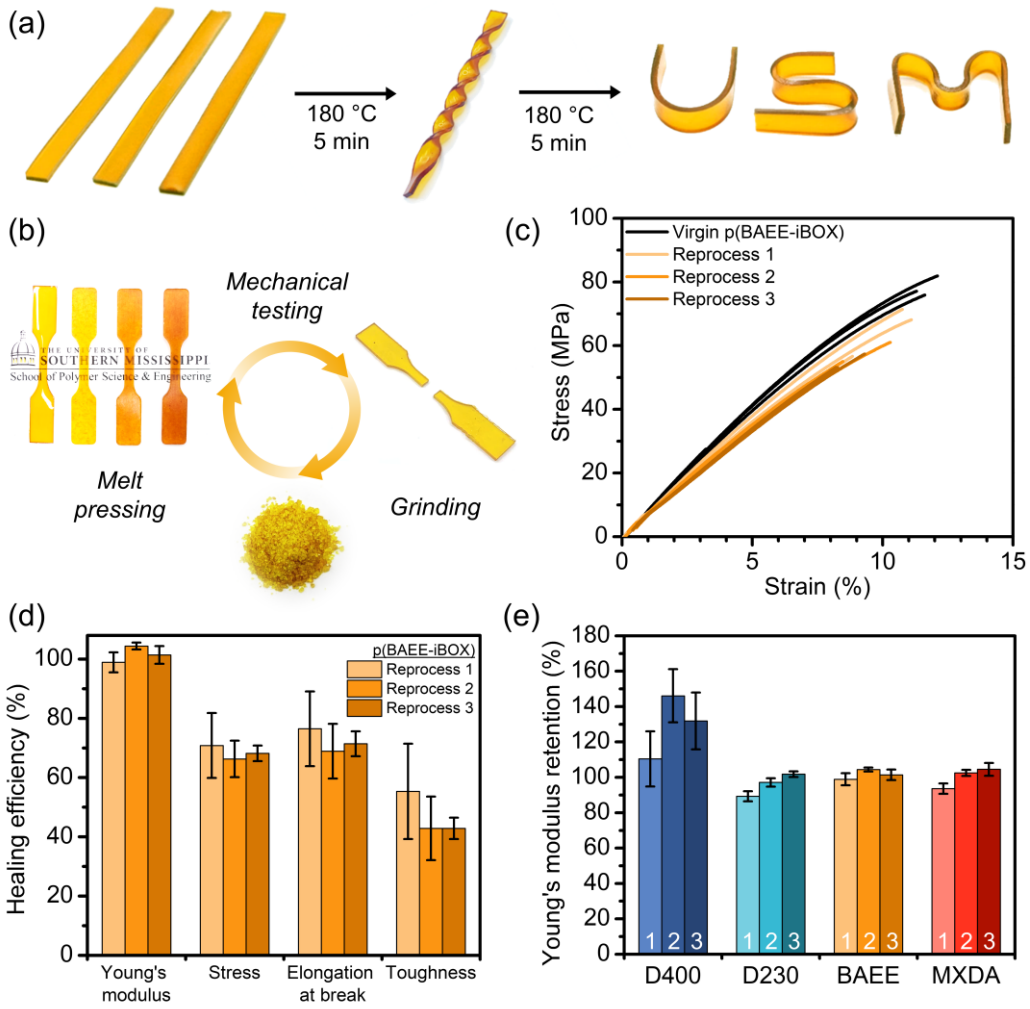

Figure 8. (a) Malleability of p(BAEE-iBOX) achieved by heating above Tv. (b) Reprocessing lifecycle of p(iBOX) networks. (b) Stress vs. strain curves of p(BAEE-iBOX) after reprocessing (c) Healing efficiency for p(BAEE-iBOX) through repeated reprocessing. (d) Retention of Young's modulus for all p(iBOX) networks through 3 reprocessing cycles.

irreversible damage caused to permanent, non-dynamic bonds, resulting in defects within the reprocessed networks.[70] The rubbery p(D400-iBOX) network demonstrated increases in modulus and tensile strength upon reprocessing (Fig. 8d & fig. S27†) which suggested that self-strengthening may have occurred through chain alignment from mechanical training or through the formation of additional crosslinks, both of which have been reported in low T_g dynamic networks.[81,82] The p(MXDA-iBOX) network demonstrated the lowest property retention through reprocessing (Table S6 & Fig. S30†) which was due to the high crosslink density and the rigidity of the aromatic backbone. Specifically, the high crosslink density and rigidity of the p(MXDA-iBOX) network prevented sufficient bond exchange to reform a complete covalent network, resulting in defects that lead to embrittlement. Nevertheless, the repeated reprocessing of all p(iBOX) networks demonstrated the potential of dynamic imine exchange for enabling the design of mechanically recyclable polybenzoxazine networks.

The ability of the p(iBOX) networks to undergo self-healing without application of external force was investigated by conducting scratch healing tests. Samples of each network were scratched with a razor blade and were placed in an oven preheated to 180 °C for various time intervals. The p(D400-iBOX) network demonstrated gradual scratch closure with increasing exposure time (Fig. S35†) and achieved an average reduction in scratch width of 66.7% after 2 hours of thermal treatment. The self-healing ability decreased in networks with higher crosslink densities (Fig. S39†), which was attributed to the increased rubbery plateau moduli resulting in insufficient network mobility required to enable bond exchange without application of external force. The inability for the highly crosslinked networks to undergo extensive self-healing at reprocessing temperatures indicated that these materials have good dimensional stability and resistance to flow without application of external force even when heated above $T_{v,eff}$.

Solvent stability and chemical degradation

The solvent stability testing indicated that all p(iBOX) networks had impressive resistance to swelling and hydrolysis in deionized water when compared to previously reported imine vitrimers,[16,41,83] demonstrating less than 2% mass gain and no discernible network dissolution after 7 days of immersion (Fig.

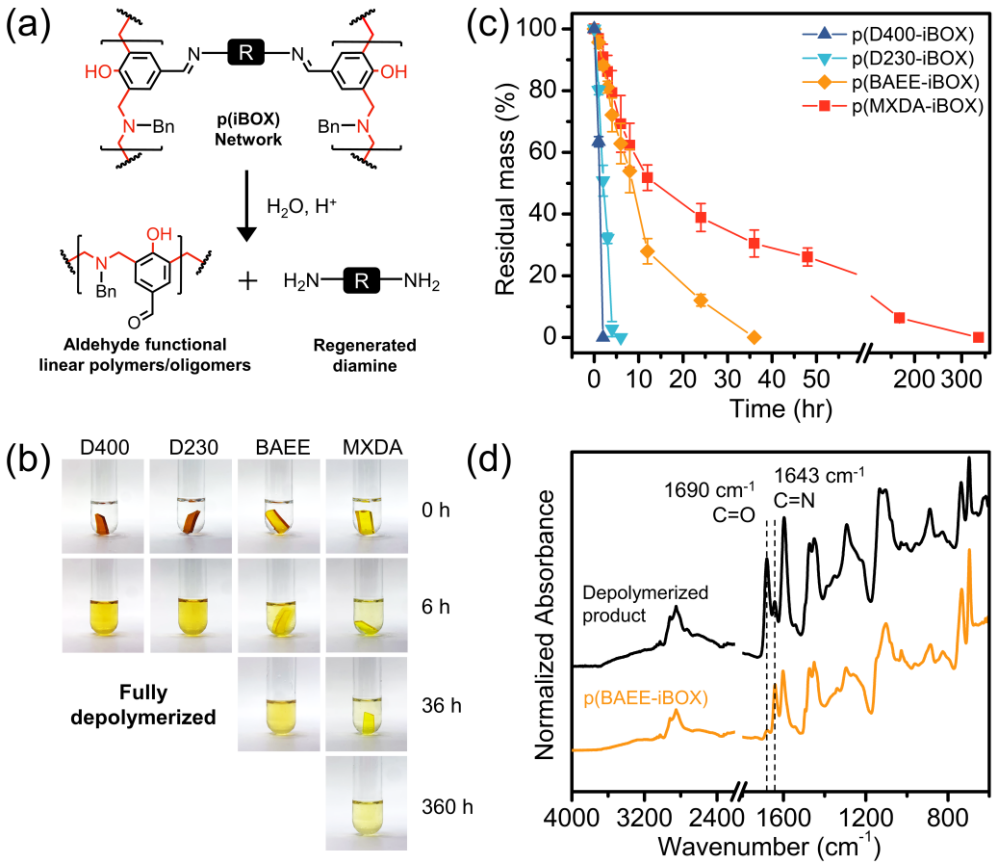

Figure 9. (a) Proposed mechanism of chemical degradation of p(iBOX) networks via imine hydrolysis. (b) Images of p(iBOX) networks in 1M HCl/THF (1:1 v/v) solution at 25 °C showing full network dissolution. (c) Residual mass vs. time curves of p(iBOX) networks in a 1M HCl /THF (1:1 v/v) solution at 25 °C. (d) FTIR spectra of p(BAEE-iBOX) network and the isolated depolymerization product after neutralizing, filtering, and drying.

S40†). The low T_g of the p(D400-iBOX) network made it susceptible to solution ingress, resulting in over 200% swelling in organic solvents such as toluene and DMF. The increased crosslink density of the p(D230-iBOX) network imparted improved stability and reduced the degree of swelling (Table S7†). Interestingly, both propylene oxide based p(iBOX) networks underwent significant mass loss in both THF and $CHCl_3$, which suggested that swelling mediated bond exchange occurred, permitting the formation of loops and other soluble network fragments which effectively reduced the gel fraction.[9,55] The p(MXDA-iBOX) network demonstrated the best solvent resistance, with mass change remaining below 2% in all tested solvents.

Based on the hydrolytic resistance of the p(iBOX) networks, degradation studies were conducted in a solution of 1M HCl and THF (1:1 v/v). The inclusion of a miscible organic solvent is often employed to promote solution ingress into the network and to aid in solubilizing the resulting macromolecular depolymerization products.[60,84] All p(iBOX) networks underwent full dissolution in the 1M HCl/THF solution at 25 °C and yielded homogenous transparent solutions (Fig. 9b). The propylene oxide networks, p(D400-iBOX) and p(D230-iBOX), rapidly decomposed within 6 h, while the ethylene oxide network, p(BAEE-iBOX), required 36 hours (Fig. 9c). The high crosslink density and solvent resistance of the p(MXDA-BOX) significantly diminished the rate of degradation and required 360 h of exposure to achieve full dissolution. Increasing the temperature to 50 °C resulted in accelerated rates of degradation, with all networks achieving full dissolution within 24 h (Fig. S41†). The proposed network degradation by imine hydrolysis (Fig. 9a) would result in the formation of an aldehyde-functionalized phenolic macromolecular component and the regenerated diamine. Upon full dissolution of the p(BAEE-iBOX) network, the depolymerized product was isolated by neutralizing the solution, resulting in the formation of a yellow precipitate. FTIR spectroscopy of the isolated degradation product indicated the significant reduction of the imine peak (-CH=N-, 1643 cm^{-1}) and the reappearance of the characteristic aldehyde peak (-CHO, 1690 cm^{-1}), which confirmed the hydrolysis of imine bonds was responsible for the network degradation (Fig. 9d).

Conclusions

This study demonstrated the solvent-free preparation of dynamic imine vitrimers by employing orthogonal benzoxazine ROP. The synthesis of these dynamic networks was achieved by preparing an aldehyde-functional BOX precursor which underwent subsequent solvent-free reactions with a series of diamines to form melt processable imine vitrimer precursors.

The chemical structures of the aldehyde-functional BOX precursor and the resulting iBOX monomers were confirmed by NMR and FTIR spectroscopy. Polymerization of the iBOX monomers was assessed by conducting DSC and rheology, which illustrated tailorable rheological profiles that imparted impressive monomer melt processability prior to polymerization. Formation of the dynamic network was achieved by conducting the condensate-free polymerization of the BOX moieties. The resulting vitrimer properties were highly tunable based on the employed linking diamine, achieving T_g ranging from 34 to 160 °C and tensile strength ranging from 9.7 to 80 MPa. The dynamic properties of the p(iBOX) networks were investigated by stress relaxation experiments, exhibiting rapid relaxation times (< 30 s at 180 °C), which were attributed to catalyst-free imine metathesis reactions. The measured imine exchange activation energy (70 and 177 kJ/mol) was found to be largely dependent on the crosslink density of the network, resulting from diffusion limitations of dynamic moieties. The $T_{v,eff}$ was measured through non-isothermal creep and expansion TMA, where it was found that $T_{v,eff}$ identified a practical temperature for reprocessing. Creep-recovery experiments indicated that the p(iBOX) networks possessed impressive creep resistance at temperatures below $T_{v,eff}$, and demonstrated predictable strain behavior at elevated temperatures based on the crosslink density. Finally, the dynamic networks displayed efficient chemical degradation under acid conditions enabling full network dissolution. The highlighted malleability, reprocessability, and chemical degradation of the p(iBOX) networks reflects the utility of orthogonal polymerizations for designing vitrimer precursors that possess liquid monomer processability, condensate-free polymerizations, and multiple avenues for recycling the resulting covalent network. The enhanced solvent-free processability of vitrimer precursors reported in this work are expected to advance the application of imine vitrimers as alternatives to conventional thermosets.

Author Contributions

The manuscript was written through contributions of all authors. All authors have given approval to the final version of the manuscript.

Conflicts of interest

There are no conflicts to declare.

Acknowledgements

The authors gratefully acknowledge the partial support of this research from Dr. John La Scala of the US Army Research Laboratory (Award W911NF-18-2-0061).

Notes and references

1 C. J. Kloxin, T. F. Scott, B. J. Adzima and C. N. Bowman, *Macromolecules*, 2010, **43**, 2643–2653.
2 J. M. Winne, L. Leibler and F. E. Du Prez, *Polym. Chem.*, 2019, **10**, 6091–6108.
3 L. Yue, V. S. Bonab, D. Yuan, A. Patel, V. Karimkhani and I. Manas-Zloczower, *Global Challenges*, 2019, **3**, 1800076.
4 C. J. Kloxin and C. N. Bowman, *Chem. Soc. Rev.*, 2013, **42**, 7161–7173.
5 M. Podgórski, B. D. Fairbanks, B. E. Kirkpatrick, M. McBride, A. Martinez, A. Dobson, N. J. Bongiardina and C. N. Bowman, *Advanced Materials*, 2020, **32**, 1906876.
6 N. Zheng, Y. Xu, Q. Zhao and T. Xie, *Chem. Rev.*, 2021, **121**, 1716–1745.
7 T. E. Long, *Science*, 2014, **344**, 706–707.
8 V. Schenk, K. Labastie, M. Destarac, P. Olivier and M. Guerre, *Mater. Adv.*, 2022, **3**, 8012–8029.
9 B. R. Elling and W. R. Dichtel, *ACS Cent. Sci.*, 2020, **6**, 1488–1496.
10 A. Jourdain, R. Asbai, O. Anaya, M. M. Chehimi, E. Drockenmuller and D. Montarnal, *Macromolecules*, 2020, **53**, 1884–1900.
11 G. M. Scheutz, J. J. Lessard, M. B. Sims and B. S. Sumerlin, *Journal of the American Chemical Society*, 2019, **141**, 16181–16196.
12 D. Montarnal, M. Capelot, F. Tournilhac and L. Leibler, *Science*, 2011, **334**, 965–968.
13 M. Capelot, M. M. Unterlass, F. Tournilhac and L. Leibler, *ACS Macro Lett.*, 2012, **1**, 789–792.
14 J. M. Winne, L. Leibler and F. E. Du Prez, *Polym. Chem.*, 2019, **10**, 6091–6108.
15 P. R. Christensen, A. Scheuermann, K. Loeffler and B. A. Helms, *Nature Chemistry*, 2019, 7.
16 P. Taynton, K. Yu, R. K. Shoemaker, Y. Jin, H. J. Qi and W. Zhang, *Advanced Materials*, 2014, **26**, 3938–3942.
17 M. Guerre, C. Taplan, J. M. Winne and F. E. Du Prez, *Chemical Science*, 2020, **11**, 4855–4870.
18 L. Li, X. Chen, K. Jin and J. M. Torkelson, *Macromolecules*, 2018, **51**, 5537–5546.
19 W. Denissen, M. Droesbeke, R. Nicolaÿ, L. Leibler, J. M. Winne and F. E. Du Prez, *Nat Commun*, 2017, **8**, 14857.
20 R. W. Layer, *Chemical Reviews*, 1963, **63**, 489–510.
21 M. Ciaccia and S. Di Stefano, *Organic & Biomolecular Chemistry*, 2015, **13**, 646–654.
22 P. Taynton, C. Zhu, S. Loob, R. Shoemaker, J. Pritchard, Y. Jin and W. Zhang, *Polymer Chemistry*, 2016, **7**, 7052–7056.
23 K. Hong, Q. Sun, X. Zhang, L. Fan, T. Wu, J. Du and Y. Zhu, *ACS Sustainable Chem. Eng.*, 2022, acssuschemeng.1c07523.
24 S. Wang, S. Ma, Q. Li, W. Yuan, B. Wang and J. Zhu, *Macromolecules*, 2018, **51**, 8001–8012.
25 Y. Tao, L. Fang, J. Zhou, C. Wang, J. Sun and Q. Fang, *ACS Applied Polymer Materials*, 2020, **2**, 295–303.
26 Y. Shen, N. Xu, Y. A. Adraro, B. Wang, Y. Liu, W. Yuan, X. Xu, Y. Huang and Z. Hu, *ACS Sustainable Chemistry & Engineering*, 2020, **8**, 1943–1953.
27 X. Shen, Y. Ma, S. Luo, R. Tao, D. An, X. Wei, Y. Jin, L. Qiu and W. Zhang, *Mater. Adv.*, 2021, **2**, 4333–4338.
28 S. K. Schoustra, J. A. Dijksman, H. Zuilhof and M. M. J. Smulders, *Chem. Sci.*, 2021, **12**, 293–302.
29 S. K. Schoustra, T. Groeneveld and M. M. J. Smulders, *Polym. Chem.*, 2021, **12**, 1635–1642.
30 P. Taynton, H. Ni, C. Zhu, K. Yu, S. Loob, Y. Jin, H. J. Qi and W. Zhang, *Advanced Materials*, 2016, **28**, 2904–2909.

31 L. Yu, C. Zhu, X. Sun, J. Salter, H. Wu, Y. Jin, W. Zhang and R. Long, *ACS Applied Polymer Materials*, 2019, **1**, 2535–2542.
32 Y. Yang, L. Huang, R. Wu, W. Fan, Q. Dai, J. He and C. Bai, *ACS Appl. Mater. Interfaces*, 2020, **12**, 33305–33314.
33 Z. Q. Lei, P. Xie, M. Z. Rong and M. Q. Zhang, *J. Mater. Chem. A*, 2015, **3**, 19662–19668.
34 C. Zhu, C. Xi, W. Doro, T. Wang, X. Zhang, Y. Jin and W. Zhang, *RSC Adv.*, 2017, **7**, 48303–48307.
35 R. Hajj, A. Duval, S. Dhers and L. Avérous, *Macromolecules*, 2020, **53**, 3796–3805.
36 K. Liang, G. Zhang, J. Zhao, L. Shi, J. Cheng and J. Zhang, *ACS Sustainable Chem. Eng.*, 2021, **9**, 5673–5683.
37 X. Lei, Y. Jin, H. Sun and W. Zhang, *J. Mater. Chem. A*, 2017, **5**, 21140–21145.
38 K. A. Stewart, J. J. Lessard, A. J. Cantor, J. F. Rynk, L. S. Bailey and B. S. Sumerlin, *RSC Appl. Polym.*, 2023, 10.1039.D3LP00019B.
39 J. Hu, R. Mo, X. Sheng and X. Zhang, *Polym. Chem.*, 2020, **11**, 2585–2594.
40 J. Stouten, M. K. N. De Roy and K. V. Bernaerts, *Materials Today Sustainability*, 2023, **22**, 100396.
41 S. Zhao and M. M. Abu-Omar, *Macromolecules*, 2018, **51**, 9816–9824.
42 J. Stouten, G. H. M. Schnelting, J. Hul, N. Sijstermans, K. Janssen, T. Darikwa, C. Ye, K. Loos, V. S. D. Voet and K. V. Bernaerts, *ACS Appl. Mater. Interfaces*, 2023, **15**, 27110–27119.
43 X. Xu, S. Ma, J. Wu, J. Yang, B. Wang, S. Wang, Q. Li, J. Feng, S. You and J. Zhu, *Journal of Materials Chemistry A*, , DOI:10.1039/C9TA05293C.
44 S. Zhao and M. M. Abu-Omar, *Macromolecules*, 2018, **51**, 9816–9824.
45 M. Fei, Y.-C. Chang, C. Hao, L. Shao, W. Liu, B. Zhao and J. Zhang, *Composites Part B: Engineering*, 2023, **248**, 110366.
46 S. Wang, S. Ma, Q. Li, X. Xu, B. Wang and Z. Jin, *Green Chemistry*, 2019, **18**, 1484–1497.
47 R. Mo, J. Hu, H. Huang, X. Sheng and X. Zhang, *J. Mater. Chem. A*, 2019, **7**, 3031–3038.
48 H. Ishida, *Handbook of Benzoxazine Resins*, Elsevier, 2011.
49 X. Ning and H. Ishida, *Journal of Polymer Science Part A: Polymer Chemistry*, 1994, **32**, 1121–1129.
50 F. I. Anagwu, V. K. Thakur and A. A. Skordos, *Macro Materials & Eng*, 2022, 2200534.
51 A. Trejo-Machin, L. Puchot and P. Verge, *Polym. Chem.*, 2020, **11**, 7026–7034.
52 A. Adjaoud, A. Trejo-Machin, L. Puchot and P. Verge, *Polym. Chem.*, 2021, **12**, 3276–3289.
53 A. Adjaoud, L. Puchot and P. Verge, *ACS Sustainable Chem. Eng.*, 2022, **10**, 594–602.
54 A. Adjaoud, L. Puchot, C. E. Federico, R. Das and P. Verge, *Chemical Engineering Journal*, 2023, **453**, 139895.
55 Z. Zhu, S. West, H. Chen, G.-H. Lai, S. Uenuma, K. Ito, M. Kotaki and H.-J. Sue, *ACS Appl. Polym. Mater.*, 2023, **5**, 3971–3978.
56 J. Chen, X. Lu and Z. Xin, *Reactive and Functional Polymers*, 2023, 105653.
57 Z. Wen, L. Bonnaud, P. Dubois and J. Raquez, *J of Applied Polymer Sci*, 2022, **139**, 52120.
58 S. Gulyuz, Y. Yagci and B. Kiskan, *Polym. Chem.*, 2022, **13**, 3631–3638.
59 X.-L. Sha, L. Yuan, G. Liang and A. Gu, *Polymer*, 2020, **202**, 122673.
60 L. Liu, F. Wang, Y. Zhu and H. Qi, *Polymers for Advanced Techs*, 2023, **34**, 405–418.
61 H. Liu, Q.-Q. Liu, L. Tian, L.-Y. Wang, K. Xu, Q.-X. Chen and B.-L. Ou, *Reactive and Functional Polymers*, 2018, **124**, 139–148.
62 A. Van, K. Chiou and H. Ishida, *Polymer*, 2014, **55**, 1443–1451.
63 A. M. Hubbard, Y. Ren, D. Konkolewicz, A. Sarvestani, C. R. Picu, G. S. Kedziora, A. Roy, V. Varshney and D. Nepal, *ACS Appl. Polym. Mater.*, 2021, acsapm.0c01290.
64 A. M. Hubbard, Y. Ren, A. Sarvestani, C. R. Picu, V. Varshney and D. Nepal, *Polymer Testing*, 2023, **118**, 107877.
65 J. Sun, W. Wei, Y. Xu, J. Qu, X. Liu and T. Endo, *RSC Adv.*, 2015, **5**, 19048–19057.
66 J. Zong and Q. Ran, *ChemistrySelect*, 2019, **4**, 6687–6696.
67 L. Han, D. Iguchi, P. Gil, T. R. Heyl, V. M. Sedwick, C. R. Arza, S. Ohashi, D. J. Lacks and H. Ishida, *J. Phys. Chem. A*, 2017, **121**, 6269–6282.
68 M. W. Couch and C. M. Williams, *Org. Mass Spectrom.*, 1972, **6**, 21–32.
69 Q. Ran, Y. Gu and H. Ishida, in *Advanced and Emerging Polybenzoxazine Science and Technology*, Elsevier, 2017, pp. 171–204.
70 Y. Yang, Z. Xia, L. Huang, R. Wu, Z. Niu, W. Fan, Q. Dai, J. He and C. Bai, *ACS Appl. Mater. Interfaces*, 2022, **14**, 47025–47035.
71 H. Ishida, in *Handbook of Benzoxazine Resins*, Elsevier, 2011, pp. 3–81.
72 T. Takeichi, T. Kano and T. Agag, *Polymer*, 2005, **46**, 12172–12180.
73 M. Ohara, K. Yoshimoto, T. Kawauchi and T. Takeichi, *Polymer*, 2020, **202**, 122668.
74 Y. Bai, P. Yang, Y. Song, R. Zhu and Y. Gu, *RSC Adv.*, 2016, **6**, 45630–45635.
75 S. Rimdusit, C. Jubsilp, P. Kunopast and W. Bangsen, in *Handbook of Benzoxazine Resins*, Elsevier, 2011, pp. 143–155.
76 K. A. Stewart, D. P. DeLellis, J. J. Lessard, J. F. Rynk and B. S. Sumerlin, *ACS Appl. Mater. Interfaces*, 2023, **15**, 25212–25223.
77 Y. Liu, Z. Tang, J. Chen, J. Xiong, D. Wang, S. Wang, S. Wu and B. Guo, *Polymer Chemistry*, 2020, **11**, 1348–1355.
78 A. M. Hubbard, Y. Ren, C. R. Picu, A. Sarvestani, D. Konkolewicz, A. K. Roy, V. Varshney and D. Nepal, *ACS Appl. Polym. Mater.*, 2022, **4**, 4254–4263.
79 S. Wang, S. Ma, Q. Li, X. Xu, B. Wang, K. Huang, Y. Liu and J. Zhu, *Macromolecules*, 2020, **53**, 2919–2931.
80 Z. Yang, Q. Wang and T. Wang, *ACS Appl. Mater. Interfaces*, 2016, **8**, 21691–21699.
81 N. Tratnik, N. R. Tanguy and N. Yan, *Chemical Engineering Journal*, 2023, **451**, 138610.
82 C. Ma, W. Liu, X. Zhou, J. He, Z. Wang and Z. Wang, *ACS Sustainable Chem. Eng.*, 2022, **10**, 6775–6783.
83 C. Luo, Z. Lei, Y. Mao, X. Shi, W. Zhang and K. Yu, *Macromolecules*, 2018, **51**, 9825–9838.
84 X. Liu, E. Zhang, Z. Feng, J. Liu, B. Chen and L. Liang, *J Mater Sci*, 2021, **56**, 15733–15751.